

Article

# Predicting Grapevine Water Status Based on Hyperspectral Reflectance Vegetation Indices

Isabel Pôças <sup>1,2,\*</sup>, Arlete Rodrigues <sup>2</sup>, Sara Gonçalves <sup>3</sup>, Patrícia M. Costa <sup>2</sup>, Igor Gonçalves <sup>4</sup>, Luís S. Pereira <sup>1</sup> and Mário Cunha <sup>2,3</sup>

Received: 25 August 2015; Accepted: 27 November 2015; Published: 5 December 2015

Academic Editors: Clement Atzberger and Prasad S. Thenkabail

<sup>1</sup> Linking Landscape, Environment, Agriculture and Food, Instituto Superior de Agronomia, Universidade de Lisboa, Tapada da Ajuda, Lisboa 1349-017, Portugal; lspereira@isa.utl.pt

<sup>2</sup> Geo-Space Sciences Research Centre, (CICGE), Rua do Campo Alegre, Porto 4169-007, Portugal; dr.arlete@gmail.com (A.R.); patricia.malva.costa@gmail.com (P.M.C.); mcunha@mail.icav.up.pt (M.C.)

<sup>3</sup> Faculdade de Ciências da Universidade do Porto, Rua do Campo Alegre, Porto 4169-007, Portugal; up201107700@fc.up.pt (S.G.); mccunha@fc.up.pt (M.C.)

<sup>4</sup> Associação para o Desenvolvimento da Viticultura Duriense, Quinta de Sta. Maria, Apartado 137, Godim 5050-106, Portugal; igor.goncalves@advid.pt

\* Correspondence: ipocas@mail.icav.up.pt; Tel.: +351-220-402-160; Fax: +351-220-402-490

**Abstract:** Several vegetation indices (VI) derived from handheld spectroradiometer reflectance data in the visible spectral region were tested for modelling grapevine water status estimated by the predawn leaf water potential ( $\Psi_{pd}$ ). The experimental trial was carried out in a vineyard in Douro wine region, Portugal. A statistical approach was used to evaluate which VI and which combination of wavelengths per VI allows the best correlation between VIs and  $\Psi_{pd}$ . A linear regression was defined using a parameterization dataset. The correlation analysis between  $\Psi_{pd}$  and the VIs computed with the standard formulation showed relatively poor results, with values for squared Pearson correlation coefficient ( $r^2$ ) smaller than 0.67. However, the results of  $r^2$  highly improved for all VIs when computed with the selected best combination of wavelengths (optimal VIs). The optimal Visible Atmospherically Resistant Index (VARI) and Normalized Difference Greenness Vegetation Index (NDGI) showed the higher  $r^2$  and stability index results. The equations obtained through the regression between measured  $\Psi_{pd}$  ( $\Psi_{pd\_obs}$ ) and optimal VARI and between  $\Psi_{pd\_obs}$  and optimal NDGI when using the parameterization dataset were adopted for predicting  $\Psi_{pd}$  using a testing dataset. The comparison of  $\Psi_{pd\_obs}$  with  $\Psi_{pd}$  predicted based on VARI led to  $R^2 = 0.79$  and a regression coefficient  $b = 0.96$ . Similar  $R^2$  was achieved for the prediction based on NDGI, but  $b$  was smaller ( $b = 0.93$ ). Results obtained allow the future use of optimal VARI and NDGI for estimating  $\Psi_{pd}$ , supporting vineyards irrigation management.

**Keywords:** Douro region; remote sensing; handheld spectroradiometer; predawn leaf water potential; VARI index; vineyards water management

## 1. Introduction

In Mediterranean regions, where precipitation is scarce and irregularly distributed throughout the year, irrigation plays a major role in agriculture. However, there is a rising intersectoral competition for water use, which leads to an increased need for improving crop water use and productivity.

Although grapevine was traditionally non-irrigated in the Douro Valley, irrigation has recently been introduced in several areas aiming to regulate crop yield and quality. A strategy of deficit irrigation (DI) has been often adopted for vines aiming to obtain high quality grapes for wine production [1,2]. An adequate management of DI depends upon an accurate control of the crop

water status, which is often done through measurements of predawn leaf water potential ( $\Psi_{pd}$ ). The use of  $\Psi_{pd}$  for irrigation scheduling is due to the fact that a quasi equilibrium between the water potential of plants and the soil occurs before the sunrise [3,4]. Although some studies recently reported the occurrence of night-time transpiration in grapevine, resulting in incomplete predawn equilibrium between the water potential of plants and the soil, the response of such process has shown to be primarily affecting water use efficiency and is highly variable among cultivars and environmental conditions [5–9]. However, the knowledge about this effect is still limited to a small number of crops and vine cultivars. Nevertheless, the  $\Psi_{pd}$  may be considered a reliable indicator of crop water status in vineyards, thus usable for irrigation scheduling purposes [3,4,8,10]. Meanwhile, like for other plant water status indicators, the measurement of  $\Psi_{pd}$  over large areas is labor-intensive and time-consuming due to the large number of observations necessary to accurately characterize a single plot. As a consequence, non-destructive, accurate, and fast methodologies are desirable to assess crop water status and other parameters related with crop water stress or deficit [11].

In the last decades, spectral reflectance data have increasingly been used in the study of vegetation due to the strong relationship between the spectral properties of vegetation and several biophysical and biochemical attributes of vegetation, e.g., vegetation fraction, leaf pigments content, canopy water content, crop coefficients, and crop evapotranspiration (e.g., [12–17]). The corresponding spectral reflectance data are often used in the form of spectral indices, which are mathematical combinations of two or more spectral bands selected to describe the biophysical parameters of interest [18]. The rising availability of spectroradiometers, with the ability to provide hyperspectral reflectance data, *i.e.*, data collected in very narrow bandwidths (1–10 nm) and continuously over the spectral range [19], has contributed to increasing the interest in using vegetation indices (VI) based on narrowband or hyperspectral data. Most applications of such narrowband indices are focused on the study of leaf pigments concentration (e.g., [20,21]) but studies related with crop water status and plant water stress have also been published (e.g., [11,22]).

The most common reflectance based VIs related with crop water status use information from the near and mid-infrared regions because of the strong water absorption features in this region of the electromagnetic spectrum. The reflectance at 950–970 nm has proved to be useful for estimation of plant water status [23,24]. Water strongly absorbs radiation at 970 nm, 1200 nm, 1450 nm, 1930 nm, and 2500 nm bands, and these wavelengths can thus be used for estimating plant water content and water potential [4,13,18,25–27]. Several studies have focused on the use of shortwave infrared (SWIR) data to detect crop water stress (e.g., [28,29]). Alternatively, VIs derived from hyperspectral data of the visible and red-edge (sharp transition of vegetation's reflectance between red and near-infrared spectral ranges) regions of the electromagnetic spectrum have been considered for assessing crop water status and detecting crop water stress at the canopy level in crops like maize [30], barley [31], olive orchards [11], and vineyards [4,22].

The narrow band data in the visible and red-edge regions can be more easily obtained by using the commonly available field spectroradiometers or by remote sensing imagery, both from satellite sensors or unmanned aerial vehicles [22]. The use of narrow band VIs based on spectral data of the visible and red edge regions is mainly related with the content of plant pigments and the associated process of photosynthesis. Specifically, it relates with the epoxidation state of xanthophyll cycle pigments [32] and the chlorophyll fluorescence emission [33]. The first process is a proxy for water stress detection, while the second is associated with stomatal conductance under water stress conditions, as discussed by Zarco-Tejada *et al.* [22]. Thus, although there is no water absorption in the visible spectral region, several VIs based on this spectral domain have shown high correlation with crop water status and are used as its proxy due to the physiological dependence of leaf pigments on water [4,22,30,34,35].

The increasing availability of instruments providing better spectral resolution, both handheld spectroradiometers and hyperspectral sensors, allows selecting the specific wavelengths that are more sensitive to the crop-related parameters under study. For this wavelength optimization, both empirical statistical approaches and physically based methods can be used [18]. Nevertheless, in both approaches, a wide range of values of the variable of interest must be sampled in the training

set of spectra [18]. Recently, a few studies related with the assessment of crop water status have focused on this wavelength optimization process; however, only a limited number of VIs [11,22], or specific regions of the electromagnetic spectrum [13,26,27] have been considered. These studies include applications to several crops, including to vineyards. However, applications to different crop conditions and considering a larger set of VIs covering different regions of the electromagnetic spectrum in the domains of visible and near infrared are still lacking.

Considering the need to support wine growers water management practices, the objectives of the present study consisted in (i) evaluating the performance of a large set of VIs, computed with spectral data ranging from the visible to near-infrared regions, to predict grapevine  $\Psi_{pd}$ ; (ii) assessing the best narrow wavelengths combination for the several VIs (optimized formulation) using an empirical statistical approach; and (iii) comparing the performance of VIs computed with the standard formulation and the optimized formulation to estimate grapevine  $\Psi_{pd}$ . References are made to support the physiological hypotheses on the interaction of grapevine water status measured by  $\Psi_{pd}$  and the optimal VIs.

## 2. Material and Methods

### 2.1. Study Area

The research was carried out in Douro Wine Region (Figure 1), northeast Portugal, which is a well-known UNESCO World Heritage Cultural Landscape [36,37]. Viticulture is favored by the peculiar climate of Mediterranean type [38–40]. Vineyards are dominantly on sloppy and terraced landscapes that made it an unique vine landscape and favored the quality of wine produced [36,41,42]. The most common red wine varieties are the Touriga Franca, Touriga Nacional, Tinta Barroca and Tinta Roriz (*Tempranillo*), all of them native of the region [43]. The mean annual precipitation in Douro region varies from 400 to 900 mm, with an average value of 560 mm, and the mean monthly temperatures range from 5 °C to 8 °C (January) up to 21–24 °C (July). During the period April–October, the mean temperature is about 19.5 °C and thus the growing season can be defined as “warm” according to the climate maturity grouping [44]. A heavy water stress is commonly observed in summer due to the low rainfall, high vapor pressure deficit and low soil water content [45].

The study area is located in a commercial vineyard (Quinta dos Aciprestes, Real Companhia Velha) in Soutelo do Douro (41.21°N of latitude and 7.43°W of longitude; Figure 1). The vineyard has a total area of 1.17 ha, with an undulating terrain with an average slope of 25%. The soil is typical of the schist geologic complex. The vineyard was planted in 1998 adopting a bilateral Royat system, following the orientation Northeast-Southwest, with 2.2 m × 1 m plant spacing. The vines are of the cultivar Touriga Nacional, and the maximum plants height is 1.5 m. The vineyard is irrigated with a drip irrigation system with spacing of 1 m between emitters and an emitter discharge of 2 L·h<sup>-1</sup>.

The experimental plot considered in this study was divided in two blocks (Block 1 and Block 2; Figure 1). Three irrigation treatments with two replicate areas were considered in each block (Figure 1): non-irrigated (NI), irrigation treatment 1 (IT<sub>1</sub>), and irrigation treatment 2 (IT<sub>2</sub>). Irrigation was performed in three dates during the field campaign of 2014: 26 July 2014, 2 August 2014 and 8 August 2014. In the first irrigation date, both IT<sub>1</sub> and IT<sub>2</sub> treatments were equally irrigated during 8 h (33.6 mm). In the second irrigation date, just the IT<sub>2</sub> treatment was irrigated, during 4 h (16.8 mm); in the third irrigation date, water was applied for 8 h (33.6 mm) in the IT<sub>1</sub> treatment and for 6 h (25.2 mm) in IT<sub>2</sub> treatment. The irrigation dates were determined by regular measurements of predawn leaf water potential ( $\Psi_{pd}$ ) and following the management of the commercial vineyard. Field measurements were performed with two replicate sites per water regime in each block: sites A and B in block 1, and sites C and D in block 2 (Figure 1).

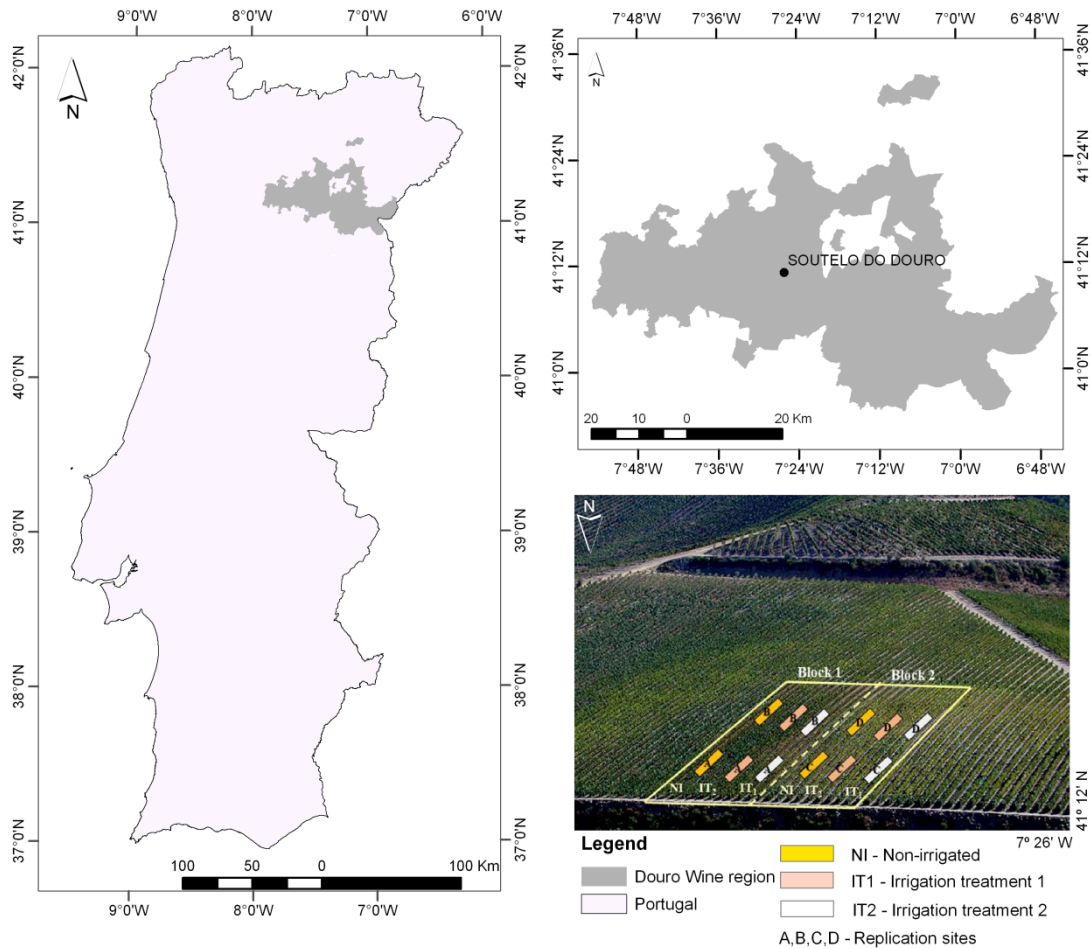


**Figure 1.** Location of the study area in the Douro Wine Region, Northeast Portugal, and identification of the experimental plot, with Blocks 1 and 2, and irrigation treatment plots.

## 2.2. Plant Water Status and Spectral Field Measurements

The water status of the vines was assessed using  $\Psi_{pd}$  observations. In grapevines, the  $\Psi_{pd}$  is highly correlated with leaf water potential measured at midday [3]. Between June and September of 2014,  $\Psi_{pd}$  was measured with a pressure chamber [46] (PMS 600, Albany, OR, USA) in six uncovered leaves in each replicate site per water regime ( $n = 12$  per water regime in each one of the blocks). Measurements were performed before sunrise in five dates through the grapevine post flowering period: 16 June 2014, 10 July 2014, 26 July 2014, 19 August 2014, and 9 September 2014.

In the same five dates, reflectance data were collected using a portable spectroradiometer (Handheld 2, ASD Instruments, Boulder, CO, USA). The spectroradiometer recorded spectral data between 325 nm and 1075 nm of the electromagnetic spectrum, with a wavelength interval of 1 nm. The spectroradiometer has a full conical angle field-of-view of 25 degrees. For the spectral signatures acquisition, the sensor was maintained 30 cm above the canopy, directed vertically downward (nadir view) in order to capture a portion of full canopy. The diameter of the spot measured in each plant was approximately 15 cm, which was smaller than the plant width (40–50 cm), hence avoiding interference of the soil. All the spectral measurements were obtained between 11 h and 13 h local time in order to minimize changes in solar zenith angle (e.g., [10,11,13,14]), in cloud free conditions, in two plants per replicate site. Thus, a total of four plants per water regime were sampled in each block. Ten repetitions of the spectral measurements were collected per plant. Before the canopy spectral data acquisition, a dark current correction was applied and the reflectance of a white standard panel (Spectralon) was measured and automatically divided by each canopy spectrum to obtain a reflectance output. These calibration procedures were automatically performed by the

spectroradiometer. Due to high noise observed at the inferior edge of the electromagnetic spectrum (<400 nm), the reflectance data of the ultraviolet region were not used. Considering the low or inexistent noise between 400 nm and 1075 nm, the raw reflectance spectral data were directly used without a smoothing pre-treatment of data through filters.

The values of  $\Psi_{pd}$  recorded in the field ( $\Psi_{pd\text{ obs}}$ ) during the year 2014 ranged from  $-0.025$  MPa to  $-0.91$  MPa, reflecting the long-term variation of  $\Psi_{pd\text{ obs}}$  registered in Douro region [45]. In addition, the recorded dataset covers all the water deficit conditions as defined by Carbonneau [47] for a vineyard: (i) none to mild water deficit conditions ( $0 \text{ MPa} > \Psi_{pd} > -0.2 \text{ MPa}$ ); (ii) mild to moderate water deficit conditions ( $-0.2 \text{ MPa} > \Psi_{pd} > -0.4 \text{ MPa}$ ); (iii) moderate to high water deficit conditions ( $-0.4 \text{ MPa} > \Psi_{pd} > -0.6 \text{ MPa}$ ); and (iv) high water deficit conditions ( $-0.6 \text{ MPa} > \Psi_{pd}$ ).

### 2.3. Selection of Vegetation Indices to Be Used as Predictors of Plant Water Status

The reflectance data provided by the spectroradiometer measurements in each date were analyzed separately. The ten records obtained for each plant were averaged. In order to define the best predictor of crop water status, several reflectance based vegetation indices (VI) currently available in the literature were computed for the five dates studied. Only VIs computed with reflectance data derived from the visible and near-infrared (NIR) regions were considered and are presented in Table 1 ([14,21,23,32,48–59]).

**Table 1.** Vegetation indices (standard formulations) considered in the current study.

Vegetation Index	Standard Formulation	Reference
Visible Atmospherically Resistant Index	$VARI = (R_{Green} - R_{Red}) / (R_{Green} + R_{Red} - R_{Blue})$	[14]
Green Index	$GI = R_{Green} / R_{Red}$	[48]
Normalized Difference Greenness Vegetation Index	$NDGI = (R_{Green} - R_{Red}) / (R_{Green} + R_{Red})$	[48]
Red Green Ratio Index	$RGRI = R_{Red} / R_{Green}$	[49]
Atmospherically resistant vegetation index (490,670,800)	$ARVI = (R_{NIR} - 2(R_{Red} - R_{Blue})) / (R_{NIR} + 2(R_{Red} - R_{Blue}))$	[50]
Simple ratio Index	$SR = R_{NIR} / R_{Red}$	[51]
Normalized Difference Vegetation Index	$NDVI = (R_{NIR} - R_{Red}) / (R_{NIR} + R_{Red})$	[52]
Soil Adjusted Vegetation Index	$SAVI = [(R_{NIR} - R_{Red}) / (R_{NIR} + R_{Red} + L)](1 + L)$	[53]
Modified Soil Adjusted Vegetation Index	$MSAVI = (2R_{NIR} + 1 - \sqrt{(2R_{NIR} + 1)^2 - 8(R_{NIR} - R_{Red})}) / 2$	[54]
Renormalized Difference Vegetation Index	$RDVI = (R_{NIR} - R_{Red}) / \sqrt{R_{NIR} + R_{Red}}$	[55]
Optimal Soil Adjusted Vegetation Index	$OSAVI = (R_{NIR} - R_{Red}) / (R_{NIR} + R_{Red} + 0.16)$	[56]
Water Index	$WI = R_{900} / R_{970}$	[23]
Photochemical Reflectance Index	$PRI = (R_{531} - R_{570}) / (R_{531} + R_{570})$	[32]
Transformed Chlorophyll Absorption in Reflectance Index	$TCARI = 3[(R_{700} - R_{670}) - 0.2(R_{700} - R_{550})(R_{700} / R_{670})]$	[57]
Modified Chlorophyll Absorption in Reflectance Index	$MCARI = [(R_{700} - R_{670}) - 0.2(R_{700} - R_{550})] \left( \frac{R_{700}}{R_{670}} \right)$	[21]
Structure Insensitive Pigment Index	$SIPI = (R_{800} - R_{445}) / (R_{800} - R_{680})$	[58]
Modified Red Edge Simple Ratio Index	$mRESR = (R_{750} - R_{445}) / (R_{705} - R_{445})$	[59]

Following the equations proposed by the original references, hereafter called standard formulations, some of the VIs were computed considering broadband regions of the electromagnetic spectrum (e.g., visible atmospherically resistant index (VARI), normalized difference greenness vegetation index (NDGI), normalized difference vegetation index (NDVI)), while others refer to specific wavelengths (water index (WI), photochemical reflectance index (PRI), transformed chlorophyll absorption in reflectance index (TCARI), modified chlorophyll absorption in reflectance (MCARI), structure insensitive pigment index (SIPI), modified red edge simple ratio index (mRESR)) (Table 1).

An analysis of the best wavelengths aimed to improve the performance of all VIs was implemented following an empirical statistical approach. Other authors have also used statistical approaches for similar purposes (e.g., [11]). In the current study, the selection of the best combination of wavelengths per VI was based on an automatic approach by testing all the possible combinations of bands, with 1 nm wavelength interval, for each VI. The full wavelengths range of the regions of the electromagnetic spectrum considered in the VI formulation (Table 1) was tested as illustrated in Figure 2. In case of the WI, PRI, TCARI, MCARI, SIPI, mRESR indices, in addition to testing the wavelengths specifically proposed in their standard formulation, the full range of wavelengths of the corresponding regions of the electromagnetic spectrum was also considered for searching the best combination of wavelengths relative to each VI. The range considered for each region of the electromagnetic spectrum was 400–450 nm for violet, 451–520 nm for blue, 521–570 nm for green, 571–700 nm for red, 681–740 nm for red edge, and 701–950 nm for near infrared (NIR). For the PRI index (Table 1), a subdivision of the green range from 521 to 545 nm and from 546 to 570 nm was considered. For the WI index (Table 1), the range from 951 to 1075 nm was also considered. For every VI, a matrix of all the possible combinations of wavelengths was built for each replicate site and associated irrigation treatment (Figure 2), in a total of six matrices per block with each element of the matrix corresponding to the VI value for a specific combination of wavelengths. A wavelength interval of 1 nm was adopted. This procedure was repeated for each date of measurements. In Figure 2, the example of a matrix for a VI combining wavelengths of the green and red regions of the electromagnetic spectrum is given,  $VI_{i,j}$ , with  $i$  and  $j$  corresponding to the green and red wavelengths (nm) respectively. A similar procedure was considered for the VIs with three bands (e.g., VARI),  $VI_{i,j,k}$ , with  $i$ ,  $j$  and  $k$  subscripts representing the wavelengths of each one of the three bands. Data from blocks 1 and 2 were analyzed separately.

$\Psi_{pd}$  was used to evaluate which VI and which combination of wavelengths per VI better assesses the crop water status. The average of the six  $\Psi_{pd\ obs}$  per replicate site was obtained for each date and analyzed against the average value of every VI for the corresponding replicate sites and for every combination of wavelengths ( $VI_{i,j}$  or  $VI_{i,j,k}$ ). A correlation analysis relating these two sets of data (VI vs.  $\Psi_{pd\ obs}$ ) was assessed for each block and the corresponding Pearson correlation coefficient ( $r$ ) was determined for each combination of wavelengths (Figure 2). Squared values of the correlation coefficient ( $r^2$ ) were considered to analyze the results of all the combinations and VIs in positive values.

To assess the consistency of the results between blocks 1 and 2, an index was computed for each wavelength combination per VI. This index, hereafter called stability index (SI), combines the average  $r^2$  obtained for blocks 1 and 2 and the respective difference:

$$\text{Stability Index (SI)} = [(r_{block\ 1}^2 + r_{block\ 2}^2)/2]/[1 + (r_{block\ 1}^2 - r_{block\ 2}^2)] \quad (1)$$

For each VI, the best combination of wavelengths was selected based on the highest values obtained for  $r^2$  and SI considering the average of the results of the two blocks, using a sorting process. The VI computed with the best combination of wavelengths was then designated optimal VI ( $VI_{opt}$ ).

The robustness of the ranges of the electromagnetic spectrum selected for each  $VI_{opt}$  was assessed by testing the full combination of bands considering wavelength intervals different from 1 nm. Therefore, the average values of reflectance obtained for wavelength intervals of 2 nm were used to compute the  $VI_{opt}$  following the same procedure described in Figure 2. A similar approach was considered for intervals of 3 nm, 4 nm, 5 nm, 6 nm, 7 nm, 8 nm, 9 nm, and 10 nm.

These tests of the full combination of bands were automatically performed using a program purposefully developed in Matlab (MathWorks, Inc.: Natick, MA, USA.).

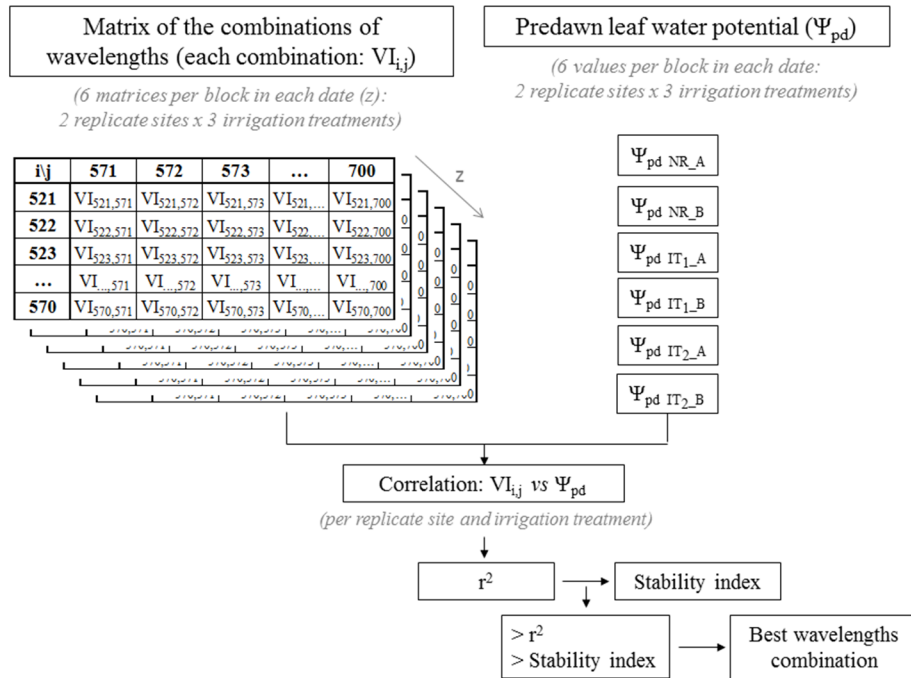


**Figure 2.** Scheme of the procedure for selecting the best wavelengths for computation of a vegetation index using a wavelengths interval of 1 nm. The scheme refers to a vegetation index combining the wavelengths of the green (i) and red (j) regions of the electromagnetic spectrum.

2.4. Statistical Analysis

The final-selected  $VI_{opt}$  were linearly regressed against the  $\Psi_{pd\ obs}$  relative to Block 1, used as parameterization dataset, and the resulting equation was adopted as the  $\Psi_{pd}$  prediction equation. Several studies considered the use of linear regression to compare crop water status and VIs (e.g., [4,22]). Moreover, a pre-assessment of the results showed an adequate adjustment of the data to this type of analysis, *i.e.*, not requiring a non-linear approach. The  $\Psi_{pd}$  prediction equation was then tested using the dataset from the block 2 ( $n = 30$ ), which was used as testing set. Subsequently, the observed and the predicted values of  $\Psi_{pd}$  relative to block 2 were compared. Additionally, a leave-one-out (LOO) cross-validation between the observed and the predicted values of  $\Psi_{pd}$  relative to block 2 was also applied. The respective results were then analyzed using various goodness-of-fit indicators to adequately assess the quality of the  $\Psi_{pd}$  predictive equation, as recommended by several authors (e.g., [60–62]).

The goodness-of-fit indicators adopted are widely used in modelling as recently analyzed by Pereira *et al.* [61]. They include [60,63]:

- (a) The determination coefficient ( $R^2$ ) of the ordinary least-squares regression between the values of  $\Psi_{pd}$  predicted with the VI predictive equation ( $\Psi_{pd\ VI}$ ) and measured ( $\Psi_{pd\ obs}$ ). A determination coefficient  $R^2$  near 1.0 indicates that most of the variance of the observed values is explained by the model (predictive equation).
- (b) The regression coefficient (b) of the linear regression through the origin relating  $\Psi_{pd\ VI}$  and  $\Psi_{pd\ obs}$ . A value of b close to 1 indicates that the predicted values are statistically close to the observed ones.
- (c) The root mean square error (RMSE) that expresses the variance of residual errors, and which may vary between zero, when a perfect match would occur, and a positive value, hopefully smaller than the mean of observations; the smaller the RMSE, the better the predictive equation.

- (d) The average absolute error (AAE), which expresses the average size of the errors of estimate.
- (e) The percent bias (PBIAS) that measures the average tendency of the predicted data to be larger or smaller than their corresponding observations. Low values indicate an accurate prediction and positive or negative values indicate the occurrence of an under- or over-estimation bias.
- (f) The absolute differences between  $\Psi_{pd\ VI}$  and  $\Psi_{pd\ obs}$  ( $|\Psi_{pd\ VI} - \Psi_{pd\ obs}|$ ) considering different classes of water deficit conditions.
- (g) The modelling efficiency (EF), proposed by Nash and Sutcliffe [64], that is used to determine the relative magnitude of the residual variance compared to the measured data variance. Values close to 1.0 indicate that the variance of residuals is much smaller than the variance of observations; contrarily, when EF is close to 0 or negative, this means that the mean is as good or better predictor than the model.

### 3. Results

#### 3.1. Selection of Predictors of Crop Water Status

The performance of the VIs, computed according to the standard formulations following the original references (Table 1) and using the optimized formulation, *i.e.*, the best combination of wavelengths (as described in Figure 2), was tested independently in blocks 1 and 2. Analyzing the correlation between the  $\Psi_{pd\ obs}$  and the VIs computed by the standard formulation (Table 2), the squared Pearson correlation ( $r^2$ ) was smaller than 0.67 ( $p < 0.001$ ) and several of the VIs (e.g., NDVI, SR, GI, WI, mRESR) presented high differences between blocks.

**Table 2.** Squared Pearson coefficient of correlation ( $r^2$ ) between the predawn leaf water potential and the vegetation indices computed by the standard formulation and by the optimized formulation (combinations of 1 nm wavelengths). Results derived for the two blocks are presented. The wavelengths used in the optimized formulation (optimal wavelengths) are presented in square brackets.

Vegetation Index	Standard Formulation		Optimized Formulation (1 nm Wavelengths)		
	Block 1 ( $n = 27$ )	Block 2 ( $n = 30$ )	Block 1 ( $n = 27$ )	Block 2 ( $n = 30$ )	Optimal Wavelengths
VARI	0.55 ***	0.58 ***	<b>0.80 ***</b>	<b>0.79 ***</b>	(520; 539; 586)
GI	0.37 ***	0.51 ***	<b>0.78 ***</b>	<b>0.81 ***</b>	(531; 587)
NDGI	0.45 ***	0.54 ***	<b>0.79 ***</b>	<b>0.79 ***</b>	(531; 587)
PRI	0.39 ***	0.39 ***	<b>0.82 ***</b>	<b>0.79 ***</b>	(545; 567)
RGRI	0.50 ***	0.54 ***	<b>0.79 ***</b>	<b>0.77 ***</b>	(531; 587)
TCARI	0.03	0.02	0.50 ***	0.55 ***	(526; 682; 650)
MCARI	0.01	0.01	0.59 ***	0.61 ***	(526; 682; 645)
ARVI	0.44 ***	0.46 ***	0.73 ***	0.66 ***	(716; 605; 520)
WI	0.00	0.59 ***	0.36 ***	0.71 ***	(943; 1038)
SR	0.04	0.29 **	0.36 ***	0.55 ***	(700; 702)
NDVI	0.09	0.20 *	0.36 ***	0.55 ***	(702; 700)
SAVI	0.23 *	0.17 *	0.42 ***	0.44 ***	(761; 700)
MSAVI	0.25 **	0.17 *	0.46 ***	0.43 ***	(761; 700)
RDVI	0.22*	0.17 *	0.37 ***	0.41 ***	(761; 700)
SIPI	0.50 ***	0.35 ***	0.64 ***	0.56 ***	(701; 700; 426)
OSAVI	0.27 **	0.21 *	0.44 ***	0.56 ***	(740; 700)
mRESR	0.31 **	0.66 ***	0.49 ***	0.73 ***	(702; 700; 426)

Significance level: \*  $p < 0.05$ ; \*\*  $p < 0.01$ ; \*\*\*  $p < 0.001$ . The formulation of the VI is presented in Table 1.

When the best combination of 1 nm wavelengths interval was considered in the computation of the VIs, the  $r^2$  increased for all the VIs (Table 2). The results presented in Table 2 for the optimized formulation correspond to the best  $r^2$  value achieved when considering the same combination of wavelengths in the computation of the optimal VI ( $VI_{opt}$ ) in both blocks. The  $VI_{opt}$  with better results were VARI, GI, red green ratio index (RGRI), NDGI, and PRI, all with  $r^2$  above 0.75 ( $p < 0.001$ ) in both blocks (Table 2). All these  $VI_{opt}$  integrate wavelength bands in the visible domain of the electromagnetic spectrum (Table 1): (i) the PRI considers data in the green region; (ii) the GI, RGRI and NDGI are two-bands indices integrating reflectance data in the green and red; and (iii) the VARI is a three-bands index including the blue, green and red regions.

The results of  $r^2$  obtained by the correlation between the  $\Psi_{pd\ obs}$  and the GI, RGRI, NDGI and PRI for all the possible combinations of 1 nm wavelengths are shown in contour maps (Figure 3). Dark blue colors represent the lower values of  $r^2$  while dark red represent the higher values, as indicated in the color-bar in Figure 3. The best combination of 1 nm wavelengths per  $VI_{opt}$ , corresponding to the highest  $r^2$  (averaged for data of the two blocks) and the highest SI, is identified in Figure 3 with black dots. The contour maps obtained for both blocks show a common area of high  $r^2$  values representing the best combinations of wavelengths for each one of the VIs (Figure 3). For the  $VARI_{opt}$  (a three-band-index), the best combination of individual bands considers the wavelengths 520 nm (Blue), 539 nm (Green) and 586 nm (Red).

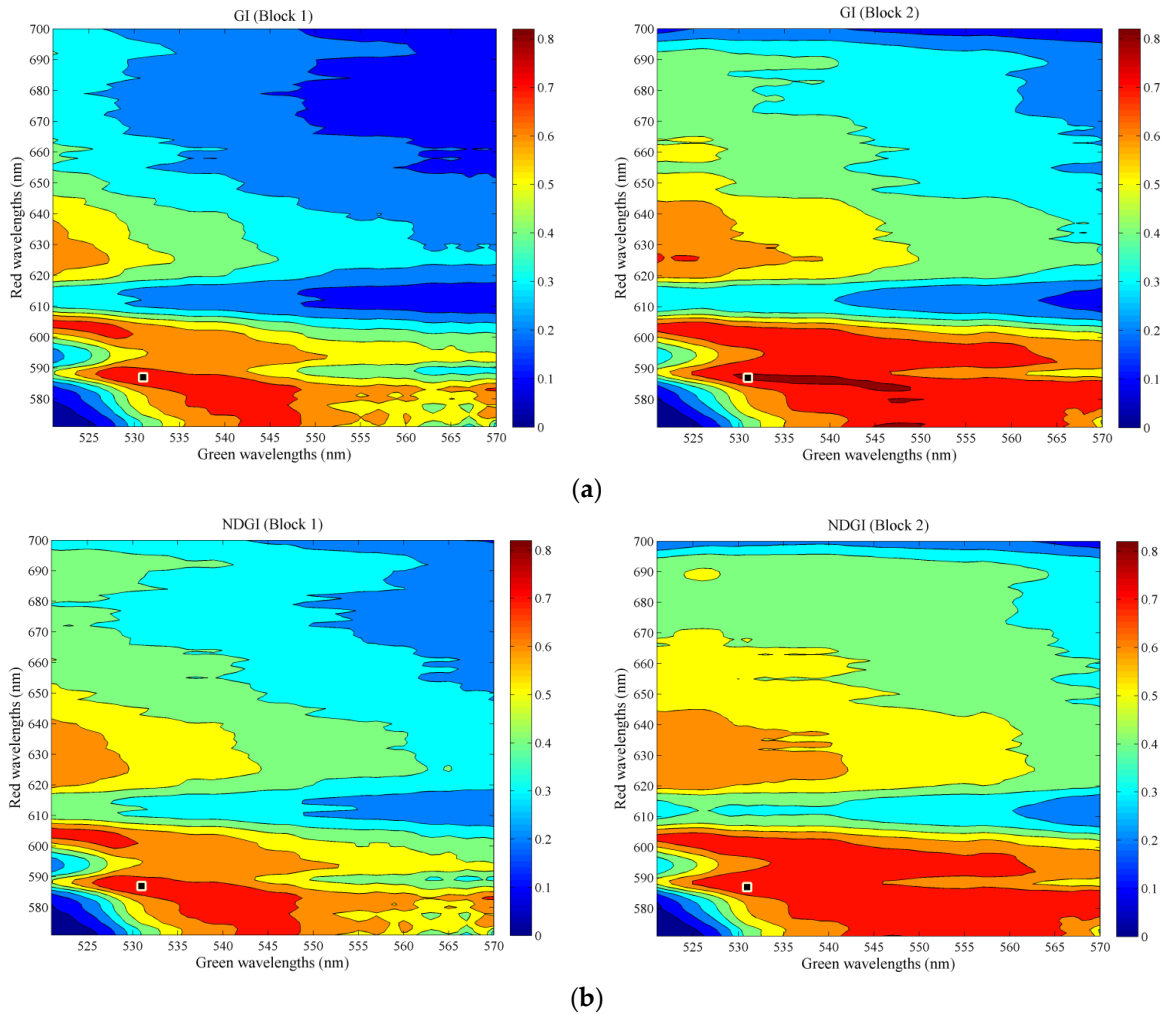
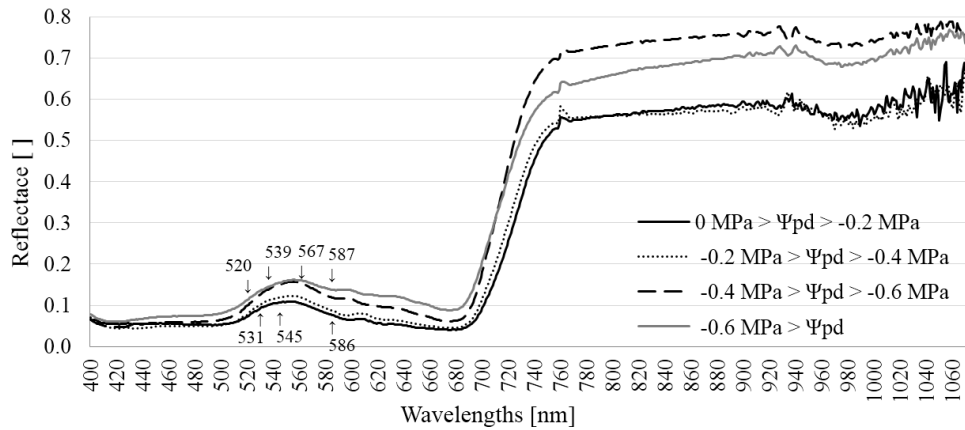


Figure 3. Cont.



wavelength intervals. The NDGI also obtained slightly better results for SI when compared with the other two-bands VIs (RGRI, GI and PRI) (Figure 5b).



**Figure 4.** Reflectance spectra signatures obtained for the different water deficit conditions defined by Carbonneau [47] for a vineyard. The vertical arrows represent the wavelengths selected for the optimal vegetation indices.

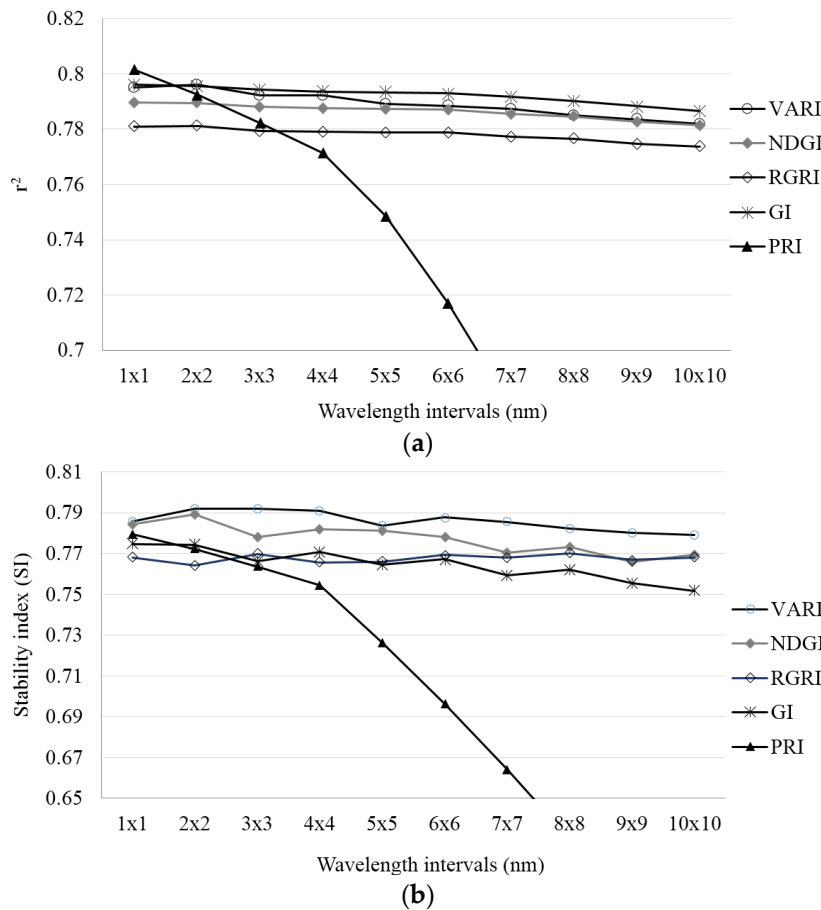


**Figure 5.** Impact of different wavelength intervals of 1 nm (1 × 1), 2 nm (2 × 2), ..., 10 nm (10 × 10) on (a) the best squared Pearson correlation coefficient ( $r^2$ ) relating the measured  $\Psi_{pd}$  and the VIs obtained with the optimized formulation; and (b) the respective stability index (SI).

### 3.2. Estimation of Leaf Water Potential ( $\Psi_{pd}$ )

Based on the previous results, the  $VARI_{opt}$  (three-bands) and the  $NDGI_{opt}$  (two-bands) were selected as predictors to estimate  $\Psi_{pd}$ . Considering the consistency of the results obtained for the several wavelength intervals (Figure 5), the results hereafter presented refer to the  $VI_{opt}$  computed using the best combination of 1 nm wavelengths.

The equations for estimating the  $\Psi_{pd}$  were determined by linear regression between  $\Psi_{pd\ obs}$  and the  $VI_{opt}$  using the parameterization dataset (data of block 1;  $n = 27$ ). The prediction equation for obtaining  $\Psi_{pd}$  from  $VARI_{opt}$  is (Figure 6a):

$$\Psi_{pd} = 3.51VARI_{opt} - 1.01 \quad (2)$$

while for  $NDGI_{opt}$ , the prediction equation is (Figure 6b):

$$\Psi_{pd} = 5.47NDGI_{opt} - 0.74 \quad (3)$$

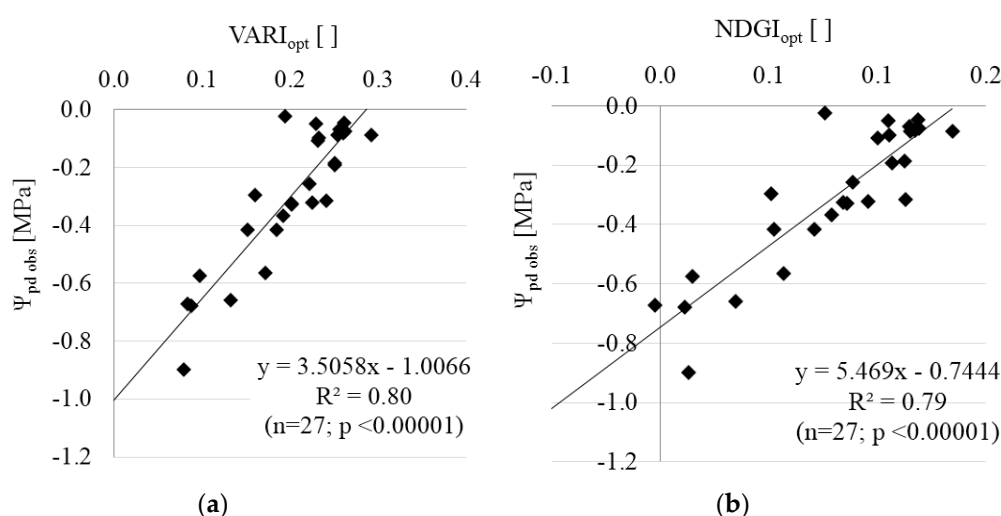


**Figure 6.** Linear regression between the observed predawn leaf water potential ( $\Psi_{pd\ obs}$ ) and the vegetation indices VARI (a) and NDGI (b) computed with the best combination of wavelengths using the parameterization dataset (block 1).

The total proportion of variance in the  $\Psi_{pd\ obs}$  explained by the  $VI_{opt}$  was 80% for  $VARI_{opt}$  and 79% for  $NDGI_{opt}$  ( $n = 27; p < 0.00001$ ).

The prediction Equations (2) and (3) were then tested to predict  $\Psi_{pd}$  using the  $VARI_{opt}$  and  $NDGI_{opt}$  computed for block 2 (testing dataset;  $n = 30$ ). The resulting  $\Psi_{pd}$  are designated  $\Psi_{pd\ VARI}$  and  $\Psi_{pd\ NDGI}$ , respectively. The goodness-of-fit indicators relative to comparing the predicted  $\Psi_{pd\ VARI}$  and  $\Psi_{pd\ NDGI}$  with the  $\Psi_{pd\ obs}$  are presented in Table 3.  $R^2 = 0.79$  were obtained for both cases, indicating a significant explanation of the  $\Psi_{pd\ obs}$  by both indices (Table 3). The regression coefficient  $b$  of 0.96 indicates a slight underestimation of  $\Psi_{pd}$  when using VARI, comparatively better than using NDGI ( $b = 0.93$ ). AAE lower than 0.1 MPa and RMSE equal to 0.12 MPa were obtained for both VIs, thus indicating small residual errors of estimation (Table 3). The PBIAS was small in both cases, indicating a slight underestimation bias of the predicted values, which was lower for  $\Psi_{pd\ VARI}$  (Table 3). The EF values were high and similar in both cases ( $EF > 0.75$ ; Table 3) indicating that the variance of residuals was much smaller than the variance of observations. Overall, these indicators show a good performance of the predictions of  $\Psi_{pd}$  with both VIs, particularly with  $VARI_{opt}$ . Similar performance of the goodness-of-fit indicators was obtained when applying the LOO cross-validation, although a slightly lower value of  $R^2$  was obtained when comparing  $\Psi_{pd\ obs}$  with both  $\Psi_{pd\ VARI}$  and  $\Psi_{pd\ NDGI}$  (Table 3).

**Table 3.** The goodness-of-fit indicators relative to predicting  $\Psi_{pd}$  with visible atmospherically resistant index (VARI)<sub>opt</sub>, normalized difference greenness vegetation index (NDGI)<sub>opt</sub> when testing the prediction equations with data of block 2 ( $n = 30$ ) and applying leave-one-out (LOO) cross-validation ( $n = 30$ ).

	Block 2		LOO Cross-Validation	
Statistics	$\Psi_{pd\ obs}$ vs. $\Psi_{pd\ VARI}$	$\Psi_{pd\ obs}$ vs. $\Psi_{pd\ NDGI}$	$\Psi_{pd\ obs}$ vs. $\Psi_{pd\ VARI}$	$\Psi_{pd\ obs}$ vs. $\Psi_{pd\ NDGI}$
R <sup>2</sup>	0.79 ( $p < 0.00001$ )	0.79 ( $p < 0.00001$ )	0.75 ( $p < 0.00001$ )	0.75 ( $p < 0.00001$ )
b	0.96	0.93	0.96	0.96
RMSE (MPa)	0.12	0.12	0.12	0.12
AAE (MPa)	0.097	0.097	0.101	0.102
PBIAS (%)	3.72	5.46	-0.52	-0.53
EF	0.76	0.77	0.75	0.75

R<sup>2</sup>—determination coefficient; b—regression coefficient; RMSE—root mean square error; AAE—average absolute error; PBIAS—percent bias; EF—model efficiency.

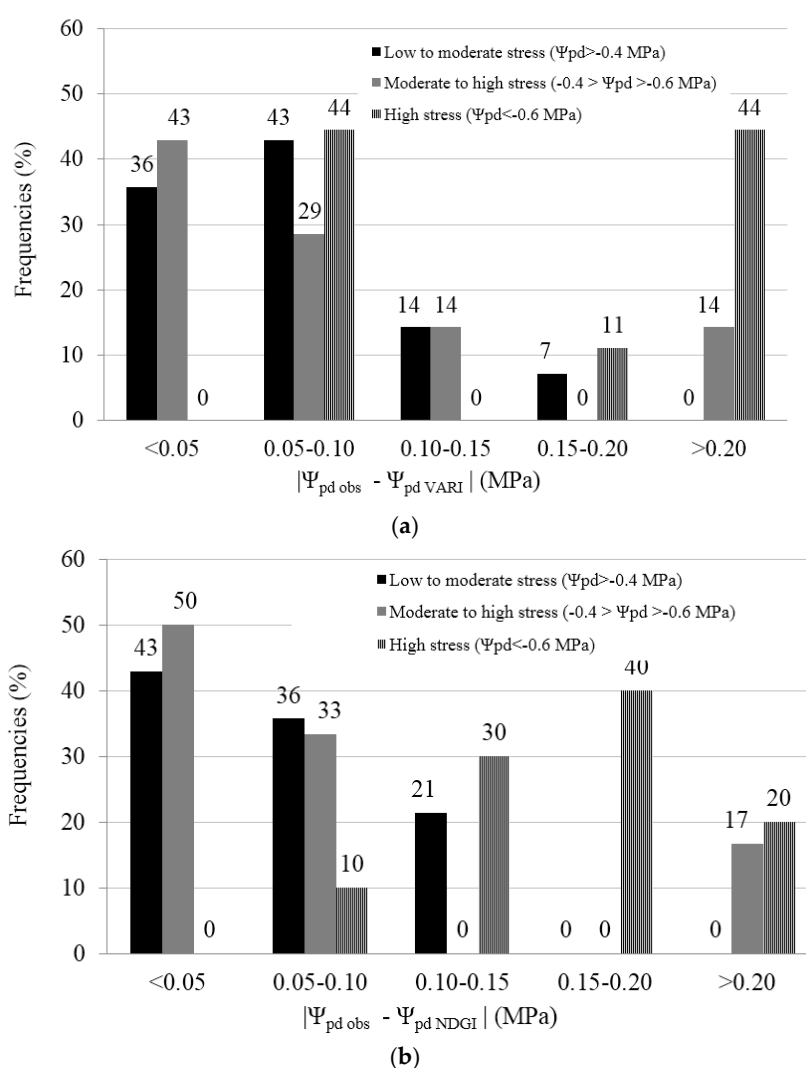


**Figure 7.** Frequencies (%) of absolute differences classes between predawn leaf water potential observed ( $\Psi_{pd\ obs}$ ) and predicted using (a) VARI ( $\Psi_{pd\ VARI}$ ) and (b) NDGI ( $\Psi_{pd\ NDGI}$ ) for the testing dataset. The value on the top of the bars stands for the frequencies.

The analysis of the absolute differences between  $\Psi_{pd\ obs}$  vs.  $\Psi_{pd\ VARI}$  ( $|\Psi_{pd\ obs} - \Psi_{pd\ VARI}|$ ) and between  $\Psi_{pd\ obs}$  vs.  $\Psi_{pd\ NDGI}$  ( $|\Psi_{pd\ obs} - \Psi_{pd\ NDGI}|$ ) for three classes of water deficit conditions is presented in Figure 7. For higher water deficits ( $\Psi_{pd} < -0.6$  MPa), the  $|\Psi_{pd\ obs} - \Psi_{pd\ VARI}|$  was smaller than 0.15 MPa in 44% of the cases and for  $|\Psi_{pd\ obs} - \Psi_{pd\ NDGI}|$  in 40%

of the cases (Figure 7). Under moderate to high water deficit ( $-0.4 > \Psi_{pd} > -0.6$  MPa) the percentage of cases with absolute differences lower than 0.15 MPa increased to 86% for  $|\Psi_{pd\ obs} - \Psi_{pd\ VARI}|$  and to 83% for  $|\Psi_{pd\ obs} - \Psi_{pd\ NDGI}|$ . In conditions of low to moderate water deficit ( $\Psi_{pd} > -0.4$  MPa),  $|\Psi_{pd\ obs} - \Psi_{pd\ NDGI}|$  were always lower than 0.15 MPa for  $|\Psi_{pd\ obs} - \Psi_{pd\ NDGI}|$  and in 93% of the cases for  $|\Psi_{pd\ obs} - \Psi_{pd\ VARI}|$  (Figure 7). The larger absolute differences ( $>0.15$  MPa) were observed for conditions of high stress ( $\Psi_{pd} < -0.6$  MPa): 55% for  $|\Psi_{pd\ obs} - \Psi_{pd\ VARI}|$  and 60% for  $|\Psi_{pd\ obs} - \Psi_{pd\ NDGI}|$  (Figure 7). These results indicate a better performance of the estimations of  $\Psi_{pd}$  VARI and  $\Psi_{pd}$  NDGI for low and moderate stress conditions in the vineyard studied.

#### 4. Discussion

In general, the results of the VIs using the standard formulation were poorly correlated with  $\Psi_{pd\ obs}$  ( $r^2 \leq 0.66$ ; Table 2). Differently, results highly improved when the VIs optimized formulation was used, *i.e.*, after selection of specific wavelengths (Table 2). Several authors also obtained better performance of VIs for estimating crop water status when narrow bands of the electromagnetic spectrum were considered [4,11,22].

In the current study, the VIs integrating information of the red and NIR spectral regions (e.g., NDVI, SR, SAVI; Table 1) were poorly correlated with  $\Psi_{pd}$  (Table 2), which was also observed by Rallo *et al.* [11] relative to olive orchards. These VIs are commonly associated with plant structural traits like leaf area index, biomass, and plant vigor (e.g., [30]) but show lower performance in the detection of physiological stress condition [65]. In addition, the results obtained by WI, specifically designed for estimation of plant water content [23], showed poor correlation with  $\Psi_{pd}$ , particularly in block 1 (Table 2). Similarly, the results of Rodríguez-Pérez [4] for the application of WI to assess water status in a vineyard (at canopy level) were not very robust. This is likely due to the low sensitivity of WI for detecting plant water content in mild drought/stress conditions [24].

The VIs integrating only information in the visible domain, in particular the optimal VARI, GI, NDGI, RGRI, and PRI (Table 1) have shown better correlations with  $\Psi_{pd\ obs}$ , with  $r^2$  values ranging from 0.77 to 0.82 in both blocks (Table 2) indicating their good performance as proxies of crop water status. This is likely due to the fact that reflectance in the visible domain is mainly governed by pigments content and composition [14,32,33], which relates with processes associated to crop water status [22]. Those five VIs have in common the integration of information in the green spectral region (Table 1). The green spectral domain is characterized by the absorption of radiation by the anthocyanins, which are water-soluble pigments associated with the resistance of plants to stresses like water deficits [15]. Differently from the other four VIs, VARI also integrates the blue band wavelengths (Table 1) that refer to a strong light absorption by carotenoids (carotenes and xanthophylls); these pigments and their proportion to chlorophyll are used as indicators for plants' physiological states and plants adaptation to stresses [66]. Furthermore, the blue band wavelengths add an atmospheric self-correction and allow a more linear relationship with the vegetation fraction [14].

VARI, GI, NDGI and RGRI are indices originally defined for measuring structural properties of vegetation and thus associated with greenness measures [18]. Their strong relationship with crop water status is potentially due to the fact that water stress manifests as an increase in green reflectance as discussed by Zygielbaum *et al.* [67]. Nevertheless, other morphological responses (e.g., leaf angle distribution, canopy geometry) as well as phenological and physiological adaptive mechanisms to stress conditions can occur and have varied effects among species [68–70], which may introduce some confounding effects on the response of these structural-oriented VIs. Additionally, factors like leaf age can also influence the spectral response thus impacting these VIs responses [70]. Contrarily, PRI is a stress/physiology-oriented hyperspectral VI [49] designed for measuring subtle decreases of reflectance around 531 nm due to changes in the xanthophyll cycle pigment activity resulting from stress conditions, including water stress conditions [32,34,68].

Rallo *et al.* [11] obtained a reasonably good prediction of  $\Psi_{pd}$  at canopy level in olive groves using optimal VIs working in the visible domain, specifically NDGI ( $R^2 = 0.57$ ,  $n = 13$ ) and GI ( $R^2 = 0.53$ ;  $n = 13$ ), however with less good results than those obtained in the current study. A good performance of VARI was also obtained by Perry and Roberts [71] when assessing water stress in

corn using data of narrow bands (10 nm width) from the AVIRIS sensor. Rodríguez-Pérez *et al.* [4] obtained good results in the estimation of water potential at canopy level using a RGRI adjusted for specific wavelengths. Differently, other authors preferred the PRI computed with the standard formulation as a good indicator of crop water stress [34,35,72]. However, issues related with viewing and illumination geometry effects, changes due to wilting or in leaf pigments content, as well as canopy structure, can affect the performance of PRI as a water stress indicator [22,34,73]. Zarco-Tejada *et al.* [22] obtained a better performance of PRI for detecting water stress in vineyard by applying a normalization of the VI, using RDVI and the  $R_{700}/R_{670}$  index. In the current study, the selection of the best wavelengths combination allowed improving the correlation of PRI with  $\Psi_{pd,obs}$ , thus increasing from an average  $r^2$  of 0.39 when using the standard formulation to a value of 0.81 using the optimized formulation (Table 2).

In the current study, the optimal NDGI, GI, and RGRI obtained the best correlations with  $\Psi_{pd,obs}$  considering the wavelengths of 531 nm and 587 nm, in the green and red domains, respectively (for wavelengths interval of 1 nm; Figure 3). As previously mentioned, the reflectance at 531 nm is considered a good indicator of stress conditions [32,66]. Moreover, the wavelength selected for the green region (531 nm) is within the range of highest sensitivity of reflectance and absorption to pigment variation [66]. In the range 530–570 nm, chlorophylls a and b play a major role in the light absorption [74]. In general, plant stress occurrence (related with a variety of causes) is indicative and closely related with chlorophyll content and losses in this pigment induce changes in leaf optical properties [75]. However, the wavelength selected in the red domain (587 nm) is not close to the range of wavelengths 680–700 nm (red-edge region) considered as reference in several studies (e.g., [11,49]), but instead is closer to the green region. In the optimized formulation of NDGI and GI for an application in olive groves, a red band around 680 nm was considered by Rallo *et al.* [11]. The difference in the wavelengths selected for these VIs may be due to variations in the leaf structure of the crops. The olive is a sclerophyllous plant, typically tolerant to drought stress, with leaves constituted by a compact mesophyll structure that reflects less light than leaves from non-sclerophyllous plants with spongy mesophyll. This is likely due to the lower hydrated cell wall-intercellular air space interfaces to reflect light [23]. In addition, the spectral region between 660 and 680 nm saturates at relatively low chlorophyll contents, thus reducing the sensitivity of this region to high chlorophyll contents of spectral VIs based on these wavelengths [59,75].

In the current study, the wavelengths selected in the  $VARI_{opt}$  were the 520 nm, 539 nm and 586 nm in the blue, green and red domains, respectively, when wavelength intervals of 1 nm were considered. The wavelengths in the regions of green and red were close to the ones selected for optimal NDGI, RGRI and GI (Figure 3), thus consistent with the results obtained for these  $VI_{opt}$ .

For the  $PRI_{opt}$ , the best combination of bands refer to the wavelengths of 545 nm and 567 nm, both in the green spectral region (Figure 3), which is different from the standard formulation (531 nm and 570 nm; Table 1). Nevertheless, various formulations of PRI, using different wavelengths, have been proposed for assessing water status in several crops, including in vineyard, using airborne data (e.g., [22,76,77]). The effect of canopy structure, viewing geometry and background on PRI may justify the diversity of formulations proposed in the literature for this VI [34]. Moreover, the overlapping effect of chlorophyll and carotenoid absorption with the spectral bands sensitive to xanthophyll pigments may potentially act as a confounding factor of PRI [22].

The reflectance of the best wavelengths selected for the five optimal VIs showed a good differentiation between classes of water deficit conditions; for conditions of low to moderate water deficit ( $\Psi_{pd} > -0.4$  MPa), which mostly occurred until around the veraison phenological stage, the values of reflectance were lower than the values for higher water deficit, which were observed for the period between veraison and ripening (Figure 4).

When the size of the wavelength intervals was evaluated for the  $VI_{opt}$  with better correlation with  $\Psi_{pd}$ ,  $VARI_{opt}$  (three-bands) and  $NDGI_{opt}$  (two-bands) have shown the best performance for the SI, with higher values for the various intervals (Figure 5b). On the contrary, the  $PRI_{opt}$  showed the worse results, both for  $r^2$  and for the SI, for wavelength intervals larger than 4 nm (Figure 5). The

lower performance of the PRI<sub>opt</sub> is likely due to the reduced number of available combinations of wavelengths that provide high  $r^2$ , when compared to the other VIs, as shown in Figure 3.

The estimation of  $\Psi_{pd}$  using the VARI<sub>opt</sub> and the NDGI<sub>opt</sub> revealed good accuracy with high values of  $R^2$  ( $R^2 = 0.79$  for data of block 2 and  $R^2 = 0.75$  for cross-validation; Table 3). Nevertheless, the results of  $\Psi_{pd\text{NDGI}}$  presented a higher underestimation than the  $\Psi_{pd\text{VARI}}$  when compared to the  $\Psi_{pd\text{obs}}$ , when directly applying data from block 2, as indicated by the regression coefficient ( $b$ ; Table 3). The  $\Psi_{pd}$  estimated with both VARI<sub>opt</sub> and NDGI<sub>opt</sub> presented low values of RMSE ( $\leq 0.12$  MPa; Table 3) and AAE ( $\leq 0.102$  MPa; Table 3) and the PBIAS was lower than 5.5% indicating a good performance of the estimation. The biases observed in the estimation of  $\Psi_{pd}$  using the VARI<sub>opt</sub> and the NDGI<sub>opt</sub> can be due to errors of  $\Psi_{pd}$  estimation but also due to errors in ground measurements of  $\Psi_{pd}$ . Regarding the latter, the occurrence of night-time transpiration can affect the  $\Psi_{pd}$  observations in some grapevine cultivars, particularly in conditions of no stress or mild stress occurrence [5,7,9]. However, irrigation is practiced only when water stress is moderate/high, thus when night-time transpiration is less important. Nevertheless, the results in this study were better than those achieved for olive groves using several VIs [11]. Contrarily, the  $R^2$  results obtained in the current study were slightly lower than the values obtained by Zarco-Tejada [22] in vineyards when correlating the leaf water potential at midday and a PRI normalized ( $R^2 = 0.82$ ;  $n = 9$ ). However, in the current study, the correlation between the normalized PRI and the  $\Psi_{pd}$  (measured at predawn and midday) did not produce good results (data not shown).

Additionally, in this study, the analysis of the absolute differences between  $\Psi_{pd\text{obs}}$  and  $\Psi_{pd\text{VI}}$  according to the frequencies showed a good performance of the model for conditions of  $\Psi_{pd} > -0.6$  MPa (Figure 7). This indicator is particularly relevant considering that a previous study indicated thresholds of  $\Psi_{pd}$  between  $-0.6$  MPa and  $-0.4$  MPa as a monitoring strategy for deficit irrigation in the field study [45].

Statistical models based on full spectrum, e.g., partial least square regression, principal component regression, support vector machine, and non-linear approaches based on artificial neural nets, have been considered to retrieve vegetation biophysical variables in alternative to the use of VIs (e.g., [13,78,79]). However, despite the outperformance of some of these methods, their operational applicability is yet limited [79]. The approach based on VIs is more easily implemented and operationally applied and the results obtained in this study demonstrated very good results for the optimal VIs.

## 5. Conclusions

A straightforward statistical approach was used to verify the adequacy of VIs computed with reflectance measurements in the visible domain aiming to detect and monitor crop water status in vineyard. Moreover, the selection of the best combination of wavelengths allowed obtaining optimal VIs.

A large set of VIs were tested and better results were obtained for the VIs integrating reflectance in the red, green, and blue spectral regions—VARI, NDGI, GI, RGRI, and PRI— particularly when the best combination wavelengths were considered. The results demonstrated a good performance of these VIs when correlated with the  $\Psi_{pd\text{obs}}$  for a period from the post-flowering until the harvest. In addition, a good consistency was obtained when data of an external dataset were tested. Moreover, the study demonstrated good results and consistency of VARI (three-bands VI) and NDGI (two-bands VI) for predicting  $\Psi_{pd}$  when several wavelength intervals were tested for the computation of the VI.

The results indicate that VARI<sub>opt</sub> and NDGI<sub>opt</sub> estimated from sensors only equipped with bands in the visible range can be used for estimating  $\Psi_{pd}$ . The use of these VI<sub>opt</sub> is more practical than the conventional measurements of  $\Psi_{pd}$ , particularly considering the increasing availability and technological improvements in handheld spectroradiometers and hyperspectral sensors, including airborne sensors. The approach presented has potential for providing an enhanced support to irrigation water management in vineyards. Nevertheless, the approach should be tested in more study areas and grape varieties in future work. Other statistical techniques based on non-linear and/or full spectrum approaches may also be tested in future work. In addition, physiological

studies regarding the response of cultivar Touriga Nacional to night-time transpiration and its impact in  $\Psi_{pd}$  may be considered in future research.

**Acknowledgments:** The first author acknowledges the FCT—Portuguese Foundation for Science and Technology for the Post-Doc research grant (SFRH/BPD/79767/2011). The authors also thank the wine company Real Companhia Velha (and its coordinator for viticulture Rui Soares) for allowing the realization of the fieldwork in Quinta dos Aciprestes.

**Author Contributions:** Isabel Pôças contributed for the current study by collecting the reflectance data, the subsequent processing of the data and the analysis of the results, and assuming the responsibility of writing the present manuscript, in collaboration with the other authors. Arlete Rodrigues was responsible for developing the program in Matlab used for selecting the best combination of bands used in the computation of the optimal vegetation indices. Sara Gonçalves and Patrícia M. Costa contributed with field work for collecting reflectance data. Igor Gonçalves was responsible for collecting and processing the predawn leaf water potential data. Luís S. Pereira and Mário Cunha contributed in the discussion of the methodology and of the results.

**Conflicts of Interest:** The authors declare no conflict of interest.

## References

1. Santesteban, L.G.; Miranda, C.; Royo, J.B. Regulated deficit irrigation effects on growth, yield, grape quality and individual anthocyanin composition in *Vitis vinifera* L. Cv. “Tempranillo”. *Agric. Water Manag.* **2011**, *98*, 1171–1179.
2. Acevedo-Opazo, C.; Ortega-Farias, S.; Fuentes, S. Effects of grapevine (*Vitis vinifera* L.) water status on water consumption, vegetative growth and grape quality: An irrigation scheduling application to achieve regulated deficit irrigation. *Agric. Water Manag.* **2010**, *97*, 956–964.
3. Williams, L.E.; Araujo, F.J. Correlations among predawn leaf, midday leaf, and midday stem water potential and their correlations with other measures of soil and plant water status in *Vitis vinifera*. *J. Am. Soc. Hortic. Sci.* **2002**, *127*, 448–454.
4. Rodríguez-Pérez, J.R.; Riaño, D.; Carlisle, E.; Ustin, S.; Smart, D.R. Evaluation of hyperspectral reflectance indexes to detect grapevine water status in vineyards. *Am. J. Enol. Vitic.* **2007**, *58*, 302–317.
5. Escalona, J.M.; Fuentes, S.; Tomás, M.; Martorell, S.; Flexas, J.; Medrano, H. Responses of leaf night transpiration to drought stress in *Vitis vinifera* L. *Agric. Water Manag.* **2013**, *118*, 50–58.
6. Flexas, J.; Galmés, J.; Gallé, A.; Gulías, J.; Pou, A.; Ribas-Carbo, M.; Tomás, M.; Medrano, H. Improving water use efficiency in grapevines: Potential physiological targets for biotechnological improvement. *Aust. J. Grape Wine Res.* **2010**, *16*, 106–121.
7. Rogiers, S.Y.; Greer, D.H.; Hutton, R.J.; Landsberg, J.J. Does night-time transpiration contribute to anisohydric behaviour in a *Vitis vinifera* cultivar? *J. Exp. Bot.* **2009**, *60*, 3751–3763.
8. Schultz, H.R.; Stoll, M. Some critical issues in environmental physiology of grapevines: Future challenges and current limitations. *Aust. J. Grape Wine Res.* **2010**, *16*, 4–24.
9. Fuentes, S.; de Bei, R.; Collins, M.J.; Escalona, J.M.; Medrano, H.; Tyerman, S. Night-time responses to water supply in grapevines (*Vitis vinifera* L.) under deficit irrigation and partial root-zone drying. *Agric. Water Manag.* **2014**, *138*, 1–9.
10. Serrano, L.; González-Flor, C.; Gorchs, G. Assessing vineyard water status using the reflectance based water index. *Agric. Ecosyst. Environ.* **2010**, *139*, 490–499.
11. Rallo, G.; Minacapilli, M.; Ciraolo, G.; Provenzano, G. Detecting crop water status in mature olive groves using vegetation spectral measurements. *Biosyst. Eng.* **2014**, *128*, 52–68.
12. Thenkabail, P.S.; Lyon, J.G.; Huete, A. Advances in hyperspectral remote sensing of vegetation and agricultural croplands. In *Hyperspectral Remote Sensing of Vegetation*; Thenkabail, P.S., Lyon, J.G., Huete, A., Eds.; CRC Press, Taylor & Francis Group: Boca Raton, FL, USA, 2012; pp. 4–35.
13. Clevers, J.G.P.W.; Kooistra, L.; Schaepman, M.E. Estimating canopy water content using hyperspectral remote sensing data. *Int. J. Appl. Earth Obs. Geoinf.* **2010**, *12*, 119–125.
14. Gitelson, A.A.; Kaufman, Y.J.; Stark, R.; Rundquist, D. Novel algorithms for remote estimation of vegetation fraction. *Remote Sens. Environ.* **2002**, *80*, 76–87.
15. Viña, A.; Gitelson, A.A. Sensitivity to foliar anthocyanin content of vegetation indices using green reflectance. *Geosci. Remote Sens. Lett. IEEE* **2011**, *8*, 464–468.

16. Pôças, I.; Paço, T.; Paredes, P.; Cunha, M.; Pereira, L. Estimation of actual crop coefficients using remotely sensed vegetation indices and soil water balance modelled data. *Remote Sens.* **2015**, *7*, 2373–2400.
17. Pôças, I.; Cunha, M.; Pereira, L.S.; Allen, R.G. Using remote sensing energy balance and evapotranspiration to characterize montane landscape vegetation with focus on grass and pasture lands. *Int. J. Appl. Earth Obs. Geoinf.* **2013**, *21*, 159–172.
18. Jones, H.G.; Vaughan, R.A. *Remote Sensing of Vegetation. Principles, Techniques, and Applications*; Oxford University Press: Oxford, UK, 2010; p. 353.
19. Thenkabail, P.S.; Teluguntla, P.; Gumma, M.K.; Dheeravath, V. Hyperspectral remote sensing for terrestrial applications. In *Remote Sensing Handbook. Land Resources Monitoring, Modeling, and Mapping with Remote Sensing*; Thenkabail, P.S., Ed.; CRC Press, Taylor and Francis Group: Boca Raton, FL, USA, 2016; pp. 201–233.
20. Zarco-Tejada, P.J.; Guillén-Climent, M.L.; Hernández-Clemente, R.; Catalina, A.; González, M.R.; Martín, P. Estimating leaf carotenoid content in vineyards using high resolution hyperspectral imagery acquired from an unmanned aerial vehicle (UAV). *Agric. For. Meteorol.* **2013**, *171–172*, 281–294.
21. Daughtry, C.S.T.; Walthall, C.L.; Kim, M.S.; de Colstoun, E.B.; McMurtrey, J.E., III, Estimating corn leaf chlorophyll concentration from leaf and canopy reflectance. *Remote Sens. Environ.* **2000**, *74*, 229–239.
22. Zarco-Tejada, P.J.; González-Dugo, V.; Williams, L.E.; Suárez, L.; Berni, J.A.J.; Goldhamer, D.; Fereres, E. A PRI-based water stress index combining structural and chlorophyll effects: Assessment using diurnal narrow-band airborne imagery and the CWSI thermal index. *Remote Sens. Environ.* **2013**, *138*, 38–50.
23. Peñuelas, J.; Filella, I.; Biel, C.; Serrano, L.; Savé, T. The reflectance at the 950–970 nm as an indicator of plant water status. *Int. J. Remote Sens.* **1993**, *14*, 1887–1905.
24. Peñuelas, J.; Pinol, J.; Ogaya, R.; Filella, I. Estimation of plant water concentration by the reflectance water index WI (R900/R970). *Int. J. Remote Sens.* **1997**, *18*, 2869–2875.
25. Roberts, D.A.; Roth, K.L.; Perroy, R.L. Hyperspectral vegetation indices. In *Hyperspectral Remote Sensing of Vegetation*; Thenkabail, P.S., Lyon, J.G., Huete, A., Eds.; CRC Press, Taylor & Francis Group: Boca Raton, FL, USA, 2012; pp. 309–327.
26. De Bei, R.; Cozzolino, D.; Sullivan, W.; Cynkar, W.; Fuentes, S.; Damberg, R.; Pech, J.; Tyerman, S. Non-destructive measurement of grapevine water potential using near infrared spectroscopy. *Aust. J. Grape Wine Res.* **2011**, *17*, 62–71.
27. González-Fernández, A.B.; Rodríguez-Pérez, J.R.; Marcelo, V.; Valenciano, J.B. Using field spectrometry and a plant probe accessory to determine leaf water content in commercial vineyards. *Agric. Water Manag.* **2015**, *156*, 43–50.
28. Berni, J.A.J.; Zarco-Tejada, P.J.; Sepulcre-Cantó, G.; Fereres, E.; Villalobos, F. Mapping canopy conductance and CWSI in olive orchards using high resolution thermal remote sensing imagery. *Remote Sens. Environ.* **2009**, *113*, 2380–2388.
29. Sepulcre-Cantó, G.; Zarco-Tejada, P.J.; Jiménez-Muñoz, J.C.; Sobrino, J.A.; de Miguel, E.; Villalobos, F.J. Detection of water stress in olive orchard with thermal remote sensing imagery. *Agric. For. Meteorol.* **2006**, *136*, 31–44.
30. Rossini, M.; Fava, F.; Cogliati, S.; Meroni, M.; Marchesi, A.; Panigada, C.; Giardino, C.; Busetto, L.; Migliavacca, M.; Amaducci, S.; Colombo, R. Assessing canopy PRI from airborne imagery to map water stress in maize. *ISPRS J. Photogramm. Remote Sens.* **2013**, *86*, 168–177.
31. Behmann, J.; Steinrücken, J.; Plümer, L. Detection of early plant stress responses in hyperspectral images. *ISPRS J. Photogramm. Remote Sens.* **2014**, *93*, 98–111.
32. Gamon, J.A.; Penuelas, J.; Field, C.B. A narrow-waveband spectral index that tracks diurnal changes in photosynthetic efficiency. *Remote Sens. Environ.* **1992**, *41*, 35–44.
33. Moya, I.; Camenen, L.; Evain, S.; Goulas, Y.; Cerovic, Z.G.; Latouche, G.; Flexas, J.; Ounis, A. A new instrument for passive remote sensing: 1. Measurements of sunlight-induced chlorophyll fluorescence. *Remote Sens. Environ.* **2004**, *91*, 186–197.
34. Suárez, L.; Zarco-Tejada, P.J.; Sepulcre-Cantó, G.; Pérez-Priego, O.; Miller, J.R.; Jiménez-Muñoz, J.C.; Sobrino, J. Assessing canopy PRI for water stress detection with diurnal airborne imagery. *Remote Sens. Environ.* **2008**, *112*, 560–575.
35. Thenot, F.; Méthy, M.; Winkel, T. The photochemical reflectance index (PRI) as a water-stress index. *Int. J. Remote Sens.* **2002**, *23*, 5135–5139.
36. Andresen, T.; de Aguiar, F.B.; Curado, M.J. The Alto Douro wine region greenway. *Landsc. Urban Plan.* **2004**, *68*, 289–303.

37. Lourenço-Gomes, L.; Rebelo, J. The Alto Douro wine region world heritage site: The complexity of a preservation program. *Rev. Tur. Patrim. Cultur.* **2012**, *10*, 3–17.
38. Gouveia, C.; Liberato, M.L.R.; DaCamara, C.C.; Trigo, R.M.; Ramos, A.M. Modelling past and future wine production in the portuguese Douro valley. *Clim. Res.* **2011**, *48*, 349–362.
39. Cunha, M.; Richter, C. Measuring the impact of temperature changes on the wine production in the Douro region using the short time Fourier transform. *Int. J. Biometeorol.* **2012**, *56*, 357–370.
40. Santos, J.A.; Grätsch, S.D.; Karremann, M.K.; Jones, G.V.; Pinto, J.G. Ensemble projections for wine production in the Douro valley of Portugal. *Clim. Chang.* **2013**, *117*, 211–225.
41. Figueiredo, T.; Poesen, J.; Ferreira, A.G.; Gonçalves, D. Runoff and soil loss from steep sloping vineyards in the Douro valley, Portugal: Rates and factors. In *Runoff Erosion, Athens, Greece, 2013*; Evelpidou, N., Cordier, S., Merino, A., Figueiredo, T.D., Centeri, C., Eds.; University of Athens: Athens, Greece, 2013; pp. 323–344.
42. Cruz, J.; Pregitzer, A.; Granja, M. *Douro River—A Golden Heritage*; Relevo, Produção Audiovisual Lda: Porto, Portugal, 2012.
43. IVDP Instituto dos Vinhos do Douro e Porto, Dados Estatísticos Sobre a Produção de Vinho do Douro e Porto na Região Demarcada do Douro. Available online: <http://www.ivdp.pt/statistics> (accessed on 21 July 2015).
44. Jones, G.V. Climate changes and the global wine industry. In Proceedings of the 13th Australian Wine Industry Technical Conference, Adelaide, Australia, 28 July–2 August 2007.
45. Alves, F.; Costa, J.; Costa, P.; Correia, C.; Gonçalves, B.; Soares, R.; Moutinho-Pereira, J. Grapevine water stress management in Douro region: Long-term physiology, yield and quality studies in cv. Touriga nacional. In Proceedings of the 18th International Symposium GiESCO, Porto, 7–11 July 2013; Portugal, Faculdade de Ciências da Universidade do Porto: Porto, Portugal, 2013.
46. Scholander, P.F.; Hammel, H.T.; Bradstreet, E.D.; Hemmingsen, E.A. Sap pressure in vascular plants. *Science* **1965**, *148*, 339–346.
47. Carbonneau, A. Irrigation, vignoble et produit de la vigne. In *Traité D'irrigation. Chapitre iv. Aspects Qualitatifs*; Tiercelin, J.R., Ed.; Lavoisier Tec et Doc: Paris, France, 1998; pp. 257–298.
48. Chamard, P.; Courel, M.F.; Docouso, M.; Guénégo, M.C.; LeRhun, J.; Levasseur, J.; Togola, M. Utilisation des bandes spectrales du vert et du rouge pour une meilleure évaluation des formations végétales actives In *Téléédétection et Cartographie*; AUPELF-UREF: Sherbrooke, QC, Canada, 1991; pp. 203–209.
49. Gamon, J.A.; Surfus, J.S. Assessing leaf pigment content and activity with a reflectometer. *New Phytol.* **1999**, *143*, 105–117.
50. Kaufman, Y.J.; Tanre, D. Atmospherically resistant vegetation index (ARVI) for EOS-MODIS. *Geosci. Remote Sens. IEEE Trans.* **1992**, *30*, 261–270.
51. Birth, G.; McVey, G. Measuring the color of growing turf with a reflectance spectrophotometer. *Agron. J.* **1968**, *60*, 640–643.
52. Rouse, W.; Haas, R.; Scheel, J.; Deering, W. Monitoring vegetation systems in great plains with ERST. In Proceedings of the Third ERTS Symposium, NASA SP-351, Washington, DC, USA, 10–14 December 1973, US Government Printing Office: Washington, DC, USA, 1973; pp. 309–317
53. Huete, A.R. A soil-adjusted vegetation index (SAVI). *Remote Sens. Environ.* **1988**, *25*, 295–309.
54. Qi, J.; Chehbouni, A.; Huete, A.R.; Kerr, Y.H.; Sorooshian, S. A modified soil adjusted vegetation index. *Remote Sens. Environ.* **1994**, *48*, 119–126.
55. Roujean, J.; Breon, F. Estimating PAR absorbed by vegetation from bidirectional reflectance measurements. *Remote Sens. Environ.* **1995**, *51*, 375–384.
56. Rondeaux, G.; Steven, M.; Baret, F. Optimization of soil-adjusted vegetation indices. *Remote Sens. Environ.* **1996**, *55*, 95–107.
57. Haboudane, D.; John, R.; Millera, J.R.; Tremblay, N.; Zarco-Tejada, P.J.; Dextraze, L. Integrated narrow-band vegetation indices for prediction of crop chlorophyll content for application to precision agriculture. *Remote Sens. Environ.* **2002**, *81*, 416–426.
58. Peñuelas, J.; Baret, F.; Filella, I. Semi-empirical indices to assess carotenoids/chlorophyll a ration from leaf spectral reflectance. *Photosynthetica* **1995**, *31*, 221–230.
59. Sims, D.A.; Gamon, J.A. Relationships between leaf pigment content and spectral reflectance across a wide range of species, leaf structures and developmental stages. *Remote Sens. Environ.* **2002**, *81*, 337–354.

60. Moriasi, D.N.; Arnold, J.G.; Van-Liew, M.W.; Bingner, R.L.; Harmel, R.D.; Veith, T.L. Model evaluation guidelines for systematic quantification of accuracy in watershed simulations. *Trans. ASABE* **2007**, *50*, 885–900.
61. Pereira, L.S.; Paredes, P.; Rodrigues, G.C.; Neves, M. Modeling malt barley water use and evapotranspiration partitioning in two contrasting rainfall years. Assessing AquaCrop and SIMDualKC models. *Agric. Water Manag.* **2015**, *159*, 239–254.
62. Tedeschi, L.O. Assessment of the adequacy of mathematical models. *Agric. Syst.* **2006**, *89*, 225–247.
63. Wang, X.; Williams, J.R.; Gassman, P.W.; Baffaut, C.; Izaurralde, R.C.; Jeong, J.; Kiniry, J.R. EPIC and APEX: Model use, calibration, and validation. *Trans. ASABE* **2012**, *55*, 1447–1462.
64. Nash, J.E.; Sutcliffe, J.V. River flow forecasting through conceptual models: Part 1. A discussion of principles. *J. Hydrol.* **1970**, *10*, 282–290.
65. Zarco-Tejada, P.J.; Berjón, A.; López-Lozano, R.; Miller, J.R.; Martín, P.; Cachorro, V.; González, M.R.; de Frutos, A. Assessing vineyard condition with hyperspectral indices: Leaf and canopy reflectance simulation in a row-structured discontinuous canopy. *Remote Sens. Environ.* **2005**, *99*, 271–287.
66. Gitelson, A.A. Nondestructive estimation of foliar pigment (chlorophylls, carotenoids, and anthocyanins) contents: Evaluating a semianalytical three-band model. In *Hyperspectral Remote Sensing of Vegetation*; Thenkabail, P.S., Lyon, J.G., Huete, A., Eds.; CRC Press: Boca Raton, FL, USA, 2012; pp. 141–165.
67. Zyguelbaum, A.I.; Gitelson, A.A.; Arkebauer, T.J.; Rundquist, D.C. Non-destructive detection of water stress and estimation of relative water content in maize. *Geophys. Res. Lett.* **2009**, *36*, 1–4.
68. Middleton, E.M.; Huemmrich, K.F.; Cheng, Y.-B.; Margolis, H.A. Spectral bioindicators of photosynthetic efficiency and vegetation stress. In *Hyperspectral Remote Sensing of Vegetation*; Thenkabail, P.S., Lyon, J.G., Huete, A., Eds.; CRC Press, Taylor & Francis Group: Boca Raton, FL, USA, 2012; pp. 265–288.
69. Morales, C.G.; Pino, M.T.; del Pozo, A. Phenological and physiological responses to drought stress and subsequent rehydration cycles in two raspberry cultivars. *Sci. Hortic.* **2013**, *162*, 234–241.
70. Guyot, G. Optical properties of vegetation canopies. In *Applications of Remote Sensing in Agriculture*; Steven, M.D., Clark, J.A., Eds.; Butterworths: London, UK, 1990; pp. 19–43.
71. Perry, E.M.; Roberts, D.A. Sensitivity of narrow-band and broad-band indices for assessing nitrogen availability and water stress in an annual crop. *Agron. J.* **2008**, *100*, 1211–1219.
72. Stagakis, S.; González-Dugo, V.; Cid, P.; Guillén-Climent, M.L.; Zarco-Tejada, P.J. Monitoring water stress and fruit quality in an orange orchard under regulated deficit irrigation using narrow-band structural and physiological remote sensing indices. *ISPRS J. Photogramm. Remote Sens.* **2012**, *71*, 47–61.
73. Sun, P.; Grignetti, A.; Liu, S.; Casacchia, R.; Salvatori, R.; Pietrini, F.; Loreto, F.; Centritto, M. Associated changes in physiological parameters and spectral reflectance indices in olive (*Olea europaea* L.) leaves in response to different levels of water stress. *Int. J. Remote Sens.* **2008**, *29*, 1725–1743.
74. Gitelson, A.A.; Kaufman, Y.J.; Merzlyak, M.N. Use of a green channel in remote sensing of global vegetation from EOS-MODIS. *Remote Sens. Environ.* **1996**, *58*, 289–298.
75. Carter, G.A.; Knapp, A.K. Leaf optical properties in higher plants: Linking spectral characteristics to stress and chlorophyll concentration. *Am. J. Bot.* **2001**, *88*, 677–684.
76. Hernández-Clemente, R.; Navarro-Cerrillo, R.M.; Suárez, L.; Morales, F.; Zarco-Tejada, P.J. Assessing structural effects on PRI for stress detection in conifer forests. *Remote Sens. Environ.* **2011**, *115*, 2360–2375.
77. Zarco-Tejada, P.J.; González-Dugo, V.; Berni, J.A.J. Fluorescence, temperature and narrow-band indices acquired from a UAV platform for water stress detection using a micro-hyperspectral imager and a thermal camera. *Remote Sens. Environ.* **2012**, *117*, 322–337.
78. Clevers, J.G.P.W.; van der Heijden, G.W.A.M.; Verzakov, S.; Schaepman, M.E. Estimating Grassland Biomass Using SVM Band Shaving of Hyperspectral Data. *Photogram. Eng. Remote Sens.* **2007**, *73*, 1141–1148.
79. Atzberger, C.; Guérif, M.; Baret, F.; Werner, W. Comparative analysis of three chemometric techniques for the spectroradiometric assessment of canopy chlorophyll content in winter wheat. *Comput. Electron. Agric.* **2010**, *73*, 165–173.

